EarthArXiv Preprint

Non-peer-reviewed manuscript prepared for submission to EarthArXiv. No DOI has been assigned.

Geometrical Assessment of Climate Models in the Drake Passage Using Multivariate Singular Spectrum Analysis

Alec Oshua Sahagún Rodríguez[1,*] Fabrice Lambert[2]

[1]Centro de Investigación en Ingeniería y Ciencias Aplicadas (CIICAp), Universidad Autónoma del Estado de Morelos (UAEM), Cuernavaca, Morelos, Mexico
ORCID: 0009-0000-8362-7770

[2]Instituto de Geografía, Pontificia Universidad Católica de Chile, Santiago, Chile
ORCID: 0000-0002-2192-024X

[*]Corresponding author: oshua1909@gmail.com

Peer-review status. This manuscript has not undergone formal peer review.

Version note. This corrected preprint uses a strictly common 1979–2014 period (432 monthly observations) for ERA5, CESM2, and ICON-ESM-LR. It includes revised figures, explicit finite-sample cautions, a Theiler window for nonlinear diagnostics, and a moving-window analysis designed to separate persistent differences from estimator instability.

Keywords. Drake Passage; M-SSA; nonlinear dynamics; atmospheric reanalysis; predictability; climate-model evaluation

Geometrical Assessment of Climate Models in the Drake Passage Using Multivariate Singular Spectrum Analysis

Alec Oshua Sahagún Rodríguez[1,*] and Fabrice Lambert[2]

Abstract

The Drake Passage is a narrow and unusually energetic ocean-atmosphere corridor, making it a useful place to ask whether climate products that agree in conventional statistics also organize their variability in the same way. We compared ERA5, CESM2, and ICON-ESM-LR over their strictly common historical period, 1979–2014 (432 months), using multivariate singular spectrum analysis (M-SSA) of 2-m air temperature, mean sea-level pressure, and zonal surface wind stress. Each series was standardized, smoothed with a 17-month uniform moving average, and embedded with a 24-month M-SSA window. We then estimated correlation dimension, maximum Lyapunov exponent, permutation entropy, Jensen-Shannon complexity, and dispersion of the leading M-SSA subspace. Global correlation-dimension estimates were close across the three products (4.43–4.72). ICON-ESM-LR nevertheless combined the highest ordinal entropy with the smallest three-dimensional subspace dispersion, while also giving the strongest linear agreement with ERA5 temperature. The moving-window analysis was less orderly: local estimates varied much more than the global values, and several windows produced correlation-dimension slopes that exceeded the embedding dimension and therefore could not be interpreted as intrinsic dimensions. The main result is not evidence for a particular strange attractor. Rather, it is that reduced-state geometrical diagnostics reveal differences that RMSE and correlation alone do not show, provided that scaling range, temporal dependence, and finite-sample limitations are treated explicitly.

1 Introduction

The Drake Passage is the principal open connection between South America and the Antarctic Peninsula and one of the most dynamically active gateways of the Southern Ocean. The Antarctic Circumpolar Current (ACC) is funneled through this region, while the overlying atmosphere is dominated by strong mid- and high-latitude westerlies. Flow, topography, meridional gradients, and synoptic variability interact over a relatively confined domain, producing climate variability from seasonal to interannual and longer time scales. Modern observational estimates place mean ACC transport through Drake Passage near 173 Sv, although the exact value depends on the section definition and observing period [4]. That combination of strong flow and geographical constraint makes the region a useful test bed for a question that is often secondary in model evaluation: not only whether two climate products have similar means and correlations, but whether their joint variability occupies and revisits reduced states in comparable ways.

Climate models are usually assessed with bias, root-mean-square error, correlation, variance, trends, and spatial climatologies. Those measures are indispensable because their meaning is directly tied to the physical variables being compared. They do not, however, describe every aspect of temporal organization. Two time series can correlate strongly and still differ in the ordering of their fluctuations, the states they visit, or the way nearby trajectories separate after a reduced-state reconstruction. Dynamical-systems diagnostics are therefore best viewed as a complementary layer of model evaluation, not as a replacement for conventional statistics.

The conceptual background comes from nonlinear atmospheric dynamics. Lorenz [11] showed that a low-dimensional deterministic system can be sensitive to initial conditions and can develop a nontrivial phase-space geometry. Nothing in that result implies that an observed climate record should reproduce the shape of the Lorenz attractor. The atmosphere-ocean system is forced, dissipative, multiscale, and only partially observed through aggregated variables. The useful lesson is more modest: moments and pairwise correlations may not be enough to characterize how states evolve in a nonlinear system.

Singular spectrum analysis (SSA) provides a data-adaptive way to decompose a signal through a trajectory matrix built from lagged copies of the series [17]. Its multivariate extension (M-SSA) treats several variables together and extracts coupled spatiotemporal modes. In climate applications, M-SSA has been used to identify oscillatory behavior, separate coherent variability from noise, and examine modulated signals [1, 6]. Unlike a transform built from prescribed sinusoidal basis functions, M-SSA derives its basis from the covariance structure of the trajectory matrix itself. That feature is useful when oscillations are nonstationary or shared across variables.

Once a reduced representation has been constructed, several nonlinear diagnostics can be explored. Correlation dimension looks for a scaling regime in the correlation sum and can be used as a finite-sample estimate of how densely a reconstructed space is occupied [7]. The Rosenstein method estimates the initial rate at which nearby reconstructed trajectories separate [13]. Permutation entropy summarizes the diversity of ordinal patterns [2], while Jensen-Shannon statistical complexity combines normalized entropy with the distance from an equiprobable ordinal distribution [14]. None of these quantities, on its own, proves the existence of a strange attractor in a finite climate record. Their value here is comparative: each product is passed through the same pipeline, and the resulting estimates are interpreted together with their fit quality and sensitivity to finite sampling.

The aim of this work is to compare the reduced-state organization of ERA5, CESM2, and ICON-ESM-LR in Drake Passage over a strictly common historical interval. We ask four questions. First, do the models reproduce the concentration of variance in the leading multivariate modes of ERA5? Second, can global geometrical diagnostics differ even when temperature-based linear scores agree well? Third, how stable are those diagnostics when estimated in moving windows of roughly decadal length? Finally, which differences remain plausible after accounting for estimator limitations? The methodological contribution is a reproducible combination of M-SSA, temporal-neighbor exclusion through a Theiler window, fit diagnostics, and explicit rejection of dimensional estimates that are incompatible with the embedding used.

2 Methods

2.1 Study design, data sources, and common period

We carried out a quantitative longitudinal comparison using existing climate products. ERA5 served as the reanalysis reference [8]. It was compared with two Coupled Model Intercomparison Project Phase 6 (CMIP6) models: CESM2 [3] and ICON-ESM-LR [9]. The monthly variables were 2-m air temperature (`tas`), mean sea-level pressure (`psl`), and zonal surface wind stress (`tauu`). Together they provide a compact description of thermal state, pressure-related dynamics, and mechanical forcing by the wind.

The analysis domain was 65°S–50°S and 285°E–300°E. ERA5 and CESM2 were interpolated to a regular 1.5° reference grid and then spatially averaged over the box. ICON-ESM-LR was available on its native mesh; cells inside the domain were selected and averaged before the monthly series were written. The final analysis therefore used one time series per variable and product. This is not a perfectly symmetric spatial treatment. In particular, a simple mean over native ICON cells is not identical to an area-weighted mean on a regular grid, and we retain that difference as a limitation rather than treating it as negligible.

Time alignment was performed with the NetCDF time coordinates, not by array index. Only January 1979 through December 2014 was retained, giving 432 complete monthly observations in every product. This step corrects an inconsistency in the preliminary analysis, where ERA5 extended to 2023 while historical CMIP6 runs began in 1850. The final pipeline explicitly intersected dates and required exactly 432 observations before any standardization. Each variable in each product was then standardized to zero mean and unit variance using statistics computed over 1979–2014.

2.2 Smoothing and multivariate reconstruction

To reduce the dominance of the annual cycle and place more emphasis on lower-frequency variability, we smoothed each standardized series with a 17-month uniform moving average. Reflective padding was used at the boundaries so that no months were discarded. We do not regard 17 months as a physically unique filter scale, nor as a perfect separation between seasonal and interannual variability. It is a common preprocessing choice applied identically to all three products, and its influence is considered again in the limitations.

After smoothing, the M-SSA embedding window was set to $M = 24$ months. For each variable, a trajectory matrix with $K = N - M + 1$ rows and M columns was constructed. The three matrices were concatenated in the order zonal wind stress–pressure–temperature,

$$X = [H_\tau \mid H_{\mathrm{PSL}} \mid H_T], \qquad C = \frac{X^{\mathrm{T}} X}{K}. \tag{1}$$

Residual column means were removed from X before diagonalizing C. Eigenvalues were sorted in descending order and expressed as percentages of explained variance. Principal components (PCs) were obtained by projecting the trajectory matrix onto the eigenvectors. Three PCs were used for visualization, whereas the first six were retained for the correlation-dimension calculation so that this diagnostic was not confined to the plotting space. Approximate North-rule uncertainties were computed using an effective sample size based on K/M [12]. Because lagged trajectory matrices contain substantial overlap, those bars are used only as a comparative guide rather than formal confidence intervals.

2.3 Correlation dimension and temporal-neighbor exclusion

Correlation dimension was estimated with a finite-sample implementation of the Grassberger-Procaccia approach [7]. Euclidean distances were calculated between states formed by the first six PCs. A Theiler window of 24 indices was imposed so that immediately adjacent points along the reconstructed trajectory did not dominate the correlation sum simply because of serial continuity [16]. Evaluation radii were spaced logarithmically over the lower part of the distance distribution, and a line was fitted in log-log coordinates,

$$C(r) \propto r^{D_2}, \qquad D_2 = \frac{d \log C(r)}{d \log r}. \tag{2}$$

We recorded both the fitted slope and its R^2. A large R^2 indicates approximate linearity over the chosen range, but it does not by itself establish an asymptotic fractal dimension. In particular, a fitted slope greater than the dimension of the embedding used here (six) cannot be interpreted as an intrinsic dimension. Such cases are retained as diagnostics of a failed or unresolved scaling regime rather than as physical estimates. This criterion becomes especially important in the moving-window analysis.

2.4 Maximum Lyapunov exponent

The maximum Lyapunov exponent was estimated with a Rosenstein-type procedure using the first three PCs [13]. For each state, the nearest spatial neighbor that was also sufficiently distant in time was identified, again using a 24-index Theiler window. The separation of each pair was followed over a short horizon, and the mean logarithmic distance was calculated. A line was fitted to the initial positive-growth segment,

$$\langle \ln d(m) \rangle \approx a + \lambda_{\max} m. \tag{3}$$

The slope was reported in month^{-1}, together with the fit R^2. For a smoothed, finite climate record, $\lambda_{\max} > 0$ is interpreted only as average neighbor separation over the scale and interval used here. It is not sufficient evidence of deterministic chaos. A slope with a weak linear fit is therefore treated more cautiously than a similar slope associated with a clear initial linear regime.

2.5 Ordinal entropy, statistical complexity, and leading-subspace dispersion

Permutation entropy was calculated from PC1 using ordinal patterns of order $m = 3$ and delay $\tau = 1$. For each consecutive triplet, the relative ordering of the values was recorded, producing a probability distribution over the $3! = 6$ possible patterns. Shannon entropy was normalized by $\ln 6$, placing H between 0 and 1. This formulation corrects an issue in the preliminary analysis in which the ordinal-pattern length did not match the normalization.

Jensen-Shannon complexity, C_{JS}, was calculated from the divergence between the observed ordinal distribution and the uniform distribution, combined with normalized entropy. It is useful for separating nearly periodic sequences, structured intermediate behavior, and distributions closer to maximal ordinal randomness [14]. We also defined a descriptive measure of leading-subspace dispersion,

$$D_3 = \sqrt{\lambda_1 \lambda_2 \lambda_3}, \tag{4}$$

where λ_i are the first three M-SSA eigenvalues after common preprocessing. D_3 is not a topological invariant. It simply summarizes the overall spread of variance in the leading three-dimensional subspace and is meaningful here only as a within-pipeline comparison.

2.6 Linear scores, moving windows, and visualization

The conventional linear comparison was based on standardized temperature before M-SSA smoothing. For CESM2 and ICON-ESM-LR we computed root-mean-square error relative to ERA5 and Pearson correlation. We label these metrics RMSE_T and r_T to make clear that they are temperature-only scores rather than multivariate summaries.

Temporal evolution was examined in seven 144-month (12-year) windows shifted by 48 months (4 years): 1979–1990, 1983–1994, 1987–1998, 1991–2002, 1995–2006, 1999–2010, and 2003–2014. Within each window, smoothing, M-SSA, D_2, and $\lambda_{\max}$ were recomputed with the same settings used globally. The longer windows provide far more reconstructed states than the five-year blocks used in the preliminary analysis, although they remain finite and partly overlapping. They are therefore treated as a sensitivity and evolution diagnostic rather than seven independent samples.

For three-dimensional figures, up to the last 400 reconstructed states were plotted; with 432 months and $M = 24$, this covers almost the full M-SSA trajectory. Cubic interpolation was used only to draw continuous lines and did not introduce additional temporal filtering. The "Poincaré-like" sections are deliberately exploratory: they select states satisfying $|\text{PC3}| < 0.2\sigma(\text{PC3})$ and show kernel density in the PC1–PC2 plane. Because no crossing direction is imposed, they are not formal Poincaré maps.

All calculations were performed in Python using NumPy, SciPy, pandas, xarray, and Matplotlib.

2.7 Ethics and reproducibility

No human participants, animals, or personal data were involved. ERA5 and the historical CMIP6 simulations are secondary scientific products distributed through established climate-data infrastructures. The final workflow records the analysis period, smoothing parameters, M-SSA window, Theiler window, permutation order, and moving-window length explicitly. Keeping those choices visible is important because the nonlinear diagnostics used here can change materially when the time span or reconstruction settings change.

3 Results and Discussion

3.1 Spectral structure and reduced-state geometry

The M-SSA spectra show that variance is concentrated in the leading modes in all three products, but the concentration is not the same (Figure 1). ERA5 has a first mode near 30% and a second near 20%, followed by a smaller third contribution. CESM2 is more strongly dominated by PC1, at roughly 36%. ICON-ESM-LR distributes its leading variance more evenly: PC1 and PC2 are close in magnitude, and PC3 still carries a substantial fraction. The approximate North-rule bars overlap considerably for the leading modes, so we do not treat them as proof of clean modal separation. In ICON-ESM-LR, the proximity of PC1 and PC2 is compatible with a strongly coupled pair, but confirming an oscillatory pair would require phase-quadrature and frequency analysis rather than visual inspection of the eigenvalues alone.

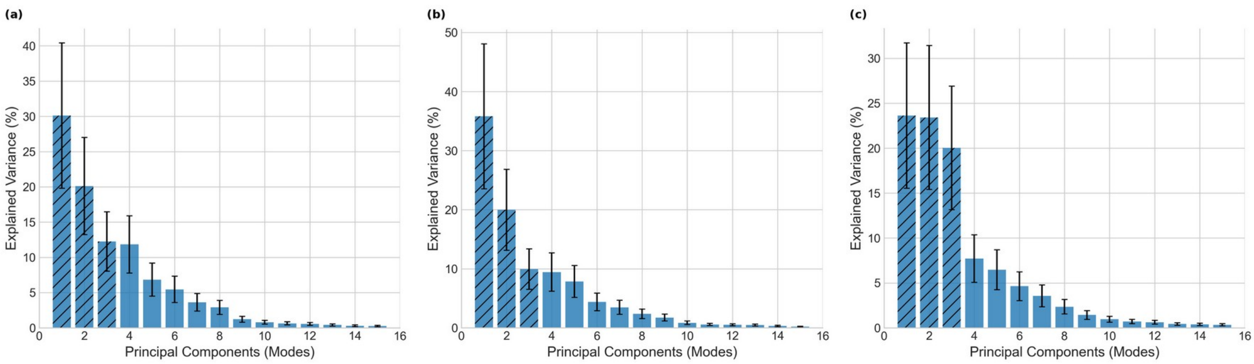

Figure 1: M-SSA explained-variance spectra for (a) ERA5, (b) CESM2, and (c) ICON-ESM-LR. The first three bars correspond to the modes used for the three-dimensional reconstruction. Vertical lines show approximate North-rule uncertainties.

The PC1–PC3 trajectories make the contrast easier to see (Figure 2). ERA5 and CESM2 move through relatively broad, irregular regions of the reduced space, with frequent changes in orientation and many apparent crossings in projection. ICON-ESM-LR is more compact and visually organized, with repeated quasi-orbital paths around a central region. We do not interpret that shape as a Lorenz attractor, or as visual proof of chaos. It simply indicates that, after identical smoothing and embedding, a larger fraction of ICON's variability is organized within a more coherent set of leading modes. Temperature coloring also shows that warm and cold filtered anomalies occur along the trajectory rather than mapping onto a single fixed branch.

The exploratory section near PC3$=0$ tells a similar story (Figure 3). ERA5 and CESM2 form broad clouds in the PC1–PC2 plane, whereas ICON-ESM-LR follows a more curved and concentrated structure. Kernel density highlights frequently visited areas, but it should not be confused with the invariant density of the original climate system. The useful point is the agreement among several descriptors: the spectral concentration, the reduced trajectory, and the smaller D_3 value all point to a more compact leading subspace in ICON. That convergence is more informative than the shape of any single plot.

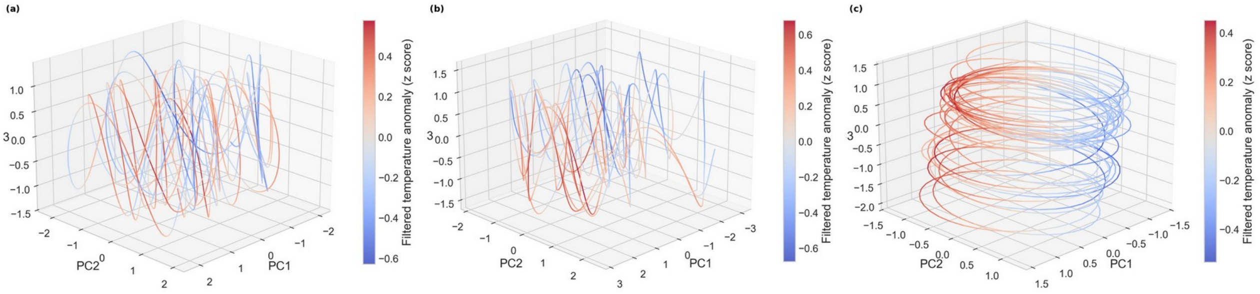

Figure 2: Reconstructed trajectories in PC1–PC2–PC3 space for (a) ERA5, (b) CESM2, and (c) ICON-ESM-LR over 1979–2014. Color denotes the standardized, filtered temperature anomaly. Interpolation was used for display only.

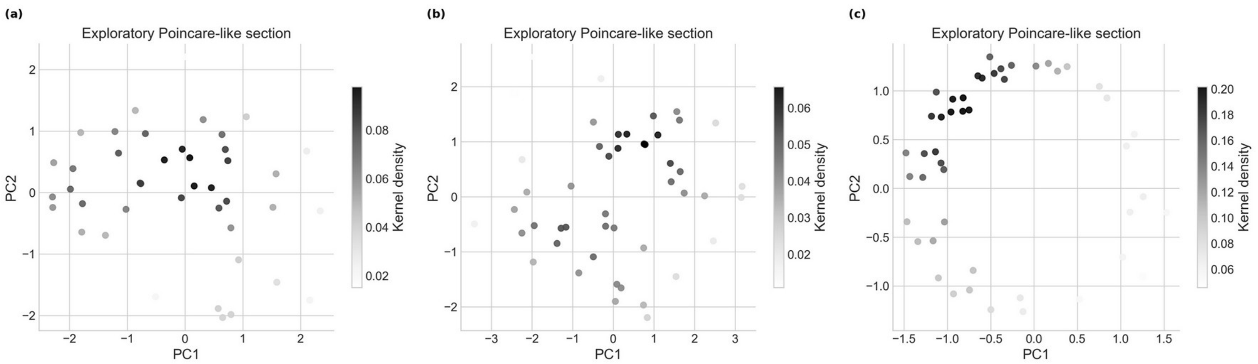

Figure 3: Exploratory Poincaré-like sections defined by states satisfying $|\mathrm{PC3}| < 0.2\sigma(\mathrm{PC3})$ for (a) ERA5, (b) CESM2, and (c) ICON-ESM-LR. Gray scale indicates kernel density in the PC1–PC2 plane. Because crossing direction is not imposed, these are descriptive sections rather than formal Poincaré maps.

3.2 Global diagnostics

Table 1 summarizes the global results. On temperature alone, ICON-ESM-LR agrees most closely with ERA5, with $\mathrm{RMSE}_T = 0.447$ in standardized units and $r_T = 0.900$. CESM2 gives $\mathrm{RMSE}_T = 0.577$ and $r_T = 0.834$. If the evaluation stopped there, ICON would be the clearer match. The reduced-state diagnostics add a different perspective: good linear agreement does not necessarily imply the same multivariate organization.

Table 1: Temperature-based linear scores and global reduced-state diagnostics for 1979–2014 (432 months). D_2 was estimated from six PCs with a Theiler window of 24 indices; $\lambda_{\max}$ used three PCs. $D_3 = \sqrt{\lambda_1\lambda_2\lambda_3}$ describes leading-subspace dispersion and is not a topological invariant.

Product	RMSE_T (z)	r_T	D_2	$\lambda_{\max}$ (month^{-1})	H_{perm}	C_{JS}	D_3
ERA5	–	–	4.426	0.1349	0.5223	0.2658	1.0469
CESM2	0.5766	0.8338	4.717	0.1306	0.4827	0.2717	1.3347
ICON-ESM-LR	0.4473	0.9000	4.533	0.1375	0.6799	0.2285	0.6990

The R^2 values for the D_2 scaling fits were 0.9984, 0.9980, and 0.9996 for ERA5, CESM2, and ICON-ESM-LR, respectively. The corresponding R^2 values for the $\lambda_{\max}$ fits were 0.6755, 0.7524, and 0.9917.

Global correlation-dimension estimates are close: 4.43 for ERA5, 4.72 for CESM2, and 4.53 for ICON-ESM-LR. The largest difference is less than 0.3. The corrected analysis therefore does not support a narrative of a global "dimensional explosion" in either model. All three log-log fits have $R^2 > 0.998$ within the selected scaling interval. That strong local linearity is useful, but it should not be mistaken for proof that the underlying climate dynamics possess a fractal dimension near 4.5. What it shows is that, under the same date range, smoothing, reconstruction, and temporal-exclusion rules, the same estimator gives similar global slopes.

The maximum Lyapunov estimates are likewise close: 0.1349 month^{-1} for ERA5, 0.1306 month^{-1} for CESM2, and 0.1375 month^{-1} for ICON-ESM-LR. The clearer difference is in the linear fit. ICON has $R^2 = 0.992$, compared with 0.676 for ERA5 and 0.752 for CESM2. The slope values themselves are therefore similar, but the initial approximately linear separation regime is much more distinct in ICON under this particular reconstruction. We interpret this as an estimator-level property of the reduced space, not as categorical evidence that one product is "more chaotic" than another.

Ordinal statistics separate the products more strongly. ICON-ESM-LR reaches $H = 0.680$, compared with 0.522 for ERA5 and 0.483 for CESM2, while its Jensen-Shannon complexity is the lowest (0.228 versus 0.266 and 0.272). In other words, PC1 in ICON samples ordinal patterns more evenly. At the same time, ICON has the smallest leading-subspace dispersion, $D_3 = 0.699$, compared with 1.047 in ERA5 and 1.335 in CESM2. A compact geometric subspace can therefore coexist with a temporally diverse ordinal sequence. That combination is precisely the kind of distinction that disappears if evaluation is restricted to RMSE and correlation.

3.3 Temporal evolution and estimator stability

The moving-window results are given in Table 2. Temporal variability is much larger than the separation among the global values. ERA5 produces D_2 slopes above six in some early windows, then falls to 3.48–3.95 in the two most recent windows. CESM2 has the largest excursions, including 9.16 in 1991–2002 and 8.04 in 2003–2014. ICON-ESM-LR remains mainly between 3.41 and 4.86, apart from 6.32 in 1979–1990. Because the D_2 reconstruction uses six dimensions, values above six cannot be interpreted as intrinsic dimensions. They instead flag windows in which the selected range does not provide a credible finite-sample scaling regime.

Table 2: Estimated correlation dimension and maximum Lyapunov exponent (month^{-1}) in 144-month moving windows shifted by 48 months. †A fitted D_2 slope above the embedding dimension (=6); retained only as a diagnostic of an unresolved scaling regime.

Window	ERA5 D_2	ERA5 λ	CESM2 D_2	CESM2 λ	ICON D_2	ICON λ
1979–1990	6.305†	0.0920	5.568	0.0878	6.316†	0.0931
1983–1994	4.732	0.0691	4.680	0.1357	4.843	0.0656
1987–1998	6.729†	0.0602	6.796†	0.0721	4.856	0.0191
1991–2002	4.925	0.0482	9.161†	0.0735	3.413	0.1011
1995–2006	4.840	0.0510	3.362	0.0297	3.805	0.0472
1999–2010	3.481	0.1267	3.814	0.0206	4.288	0.1799
2003–2014	3.952	0.0439	8.042†	0.0296	3.713	0.0940

The D_2 fits themselves are deceptively good in nearly every window: approximately 0.984–0.998 for ERA5, 0.990–0.998 for CESM2, and 0.993–0.999 for ICON. This is a useful warning. A local regression can look excellent even when the fitted slope is mathematically incompatible with the reconstructed space. R^2 alone is therefore a poor automatic criterion for identifying a scaling region. A stronger analysis would also require slope stability across radius ranges, saturation as embedding dimension increases, and consistency under resampling or surrogate-data tests.

The Lyapunov estimates show a different pattern. ICON-ESM-LR has consistently strong linear fits across all seven windows (R^2 from 0.939 to 0.999) and reaches its largest slope, 0.1799 month^{-1}, in 1999–2010. ERA5 also increases in that window to 0.1267 month^{-1}, whereas CESM2 falls to 0.0206 month^{-1}. The fit quality for ERA5 and CESM2 is less stable, reaching values as low as 0.326 and 0.298 in some windows. The most defensible temporal statement is thus not that ICON is intrinsically "more chaotic." It is that the same neighbor-separation procedure finds a more consistently linear early-growth regime in ICON over these windows.

3.4 Implications for climate-model evaluation

The corrected results expose two different kinds of agreement. At the level of standardized temperature, ICON reproduces ERA5 better than CESM2 according to both RMSE and correlation. At the level of the reduced multivariate representation, the products are not equivalent: ICON has smaller D_3, larger ordinal entropy, and lower Jensen-Shannon complexity, while CESM2 spans a broader leading subspace and has lower ordinal entropy. These differences should not automatically be labeled numerical errors. They may arise from how each model represents coupling among pressure, wind, and temperature, from different memory scales, or from differences in spatial resolution and physical parameterization.

ICON's compact geometry, together with its nearly equal first two eigenvalues, suggests a modal organization that deserves a dedicated oscillatory analysis. A natural next step would be to examine paired spatiotemporal components using lag correlations, spectra of the PCs, and Monte Carlo SSA against red-noise null models [1, 6]. That would show whether the apparent eigenvalue pairing corresponds to a statistically supported oscillation and, if so, whether it can be linked to a physical band such as interannual variability of the Southern Hemisphere westerlies or Southern Ocean modes.

The results also illustrate why the word "invariant" requires care in climate applications. D_2 and λ have rigorous definitions in idealized dynamical settings, but their finite-record estimators depend on embedding, scale range, smoothing, record length, and noise. Likewise, H and C_{JS} depend on ordinal order and delay, while D_3 depends directly on normalization and the M-SSA basis. Throughout this paper we therefore treat them as standardized comparative diagnostics. Their practical value lies in revealing structural differences while all pipeline choices are held fixed.

4 Limitations

The first limitation is record length. Thirty-six years is long enough for a homogeneous historical comparison, but it is still short for asymptotic estimates of dimension and Lyapunov exponents, especially after smoothing and lagged reconstruction. The 12-year moving windows contain even fewer effectively independent states. Because neighboring windows overlap, they should not be read as independent replicates.

The second limitation is spatial aggregation. ERA5 and CESM2 were interpolated to a common regular grid before averaging, whereas ICON-ESM-LR was reduced by a simple mean over native cells inside the box. A future version should use consistent area weights and either common regridding or a demonstrably equivalent aggregation strategy for all products. Regional means also remove gradients and local structures that may be dynamically important, so spatially resolved extensions are warranted.

Third, the 17-month smoother is a methodological choice rather than a physically unique scale. It reduces annual-cycle dominance, but it also changes autocorrelation, amplitude, and neighbor-separation time scales. Robustness should be tested with alternative windows and, ideally, with explicit seasonal-removal procedures that preserve interannual variability more transparently. The Theiler window of 24 limits immediate serial dependence, yet an optimal exclusion interval could instead be estimated from the autocorrelation time of each product.

Fourth, the scaling range for D_2 is selected automatically. The moving-window slopes above six demonstrate that a high R^2 cannot certify a fractal scaling regime. A study focused specifically on intrinsic dimension should therefore include saturation curves across embedding dimension, sensitivity to radius intervals, bootstrap uncertainty, and surrogate-series comparisons.

Finally, ERA5 is a reanalysis rather than a perfect observation. It blends observations with a forecast model and data-assimilation system and may share structural assumptions with climate models. “Reference” in this paper means reference product for comparison, not ground truth. Independent observations of winds, pressure, and ocean transport would be valuable for testing whether the reduced-state differences seen here correspond to the real system.

5 Conclusions

The corrected comparison of ERA5, CESM2, and ICON-ESM-LR uses the same 1979–2014 interval and identical analysis parameters for all three products. Once that temporal inconsistency from the preliminary analysis was removed, the global correlation-dimension and maximum-Lyapunov estimates proved remarkably similar. The revised results therefore do not support an interpretation of a global dimensional instability in ICON-ESM-LR.

The clearer differences occur in the organization of the M-SSA subspace and in ordinal-pattern statistics. ICON-ESM-LR combines the strongest temperature-based linear agreement with ERA5 with a more compact three-dimensional geometry, higher permutation entropy, and lower Jensen-Shannon complexity. CESM2 spans a broader leading subspace and has an ordinal-entropy value closer to ERA5. High linear correlation can therefore coexist with a noticeably different multivariate organization.

The moving-window analysis also shows both the promise and the limits of nonlinear diagnostics. Several local correlation-dimension fits yield slopes above the embedding dimension and must be rejected as intrinsic-dimensional estimates, even though their R^2 values are high. By contrast, ICON-ESM-LR produces a notably consistent linear neighbor-separation phase across all seven windows. Interpreting these results responsibly requires considering the estimate, its fit quality, and its mathematical plausibility together.

Taken as a set, M-SSA, correlation dimension, local neighbor divergence, ordinal entropy, and statistical complexity provide a useful complement to conventional climate-model scores when the comparison is temporally aligned and reproducible. They can expose differences in dynamical organization that are invisible to RMSE or correlation. Their use, however, should remain tied to explicit tests of scale dependence and estimator robustness rather than to claims of strange-attractor detection from finite climate records.

Data Availability

ERA5 data used in this study are available from the Copernicus Climate Data Store. Historical CESM2 and ICON-ESM-LR simulations are part of CMIP6 and are distributed through Earth System Grid Federation nodes and associated catalogs. The analysis uses monthly, spatially aggregated 2-m air temperature, mean sea-level pressure, and zonal surface wind stress for 65°S–50°S, 285°E–300°E over 1979–2014.

Author Contributions

Alec Oshua Sahagún Rodríguez: conceptualization, data curation, software, formal analysis, methodology, visualization, and original manuscript preparation. Fabrice Lambert: supervision, methodological review, and critical revision of the manuscript. Both authors reviewed the final content and approved its presentation.

Acknowledgments

The authors thank the Copernicus Climate Change Service for making ERA5 available and the CMIP6 modeling groups for providing CESM2 and ICON-ESM-LR output. We also acknowledge scientific discussions with Denisse Sciamarella and Michael Ghil, which helped shape the conceptual development of the nonlinear-dynamics analysis.

References

[1] Allen, M. R., & Robertson, A. W. (1996). Distinguishing modulated oscillations from coloured noise in multivariate datasets. *Climate Dynamics, 12*(11), 775–784. https://doi.org/10.1007/s003820050142

[2] Bandt, C., & Pompe, B. (2002). Permutation entropy: A natural complexity measure for time series. *Physical Review Letters, 88*(17), 174102. https://doi.org/10.1103/PhysRevLett.88.174102

[3] Danabasoglu, G., Lamarque, J.-F., Bacmeister, J., Bailey, D. A., DuVivier, A. K., Edwards, J., Emmons, L. K., Fasullo, J., Garcia, R., Gettelman, A., Hannay, C., Holland, M. M., Large, W. G., Lauritzen, P. H., Lawrence, D. M., Lenaerts, J. T. M., Lindsay, K., Lipscomb, W. H., Mills, M. J., Neale, R., Oleson, K. W., Otto-Bliesner, B., Phillips, A. S., Sacks, W., Tilmes, S., van Kampenhout, L., Vertenstein, M., Bertini, A., Dennis, J., Deser, C., Fischer, C., Fox-Kemper, B., Kay, J. E., Kinnison, D., Kushner, P. J., Larson, V. E., Long, M. C., Mickelson, S., Moore, J. K., Nienhouse, E., Polvani, L., Rasch, P. J., & Strand, W. G. (2020). The Community Earth System Model version 2 (CESM2). *Journal of Advances in Modeling Earth Systems, 12*(2), e2019MS001916. https://doi.org/10.1029/2019MS001916

[4] Donohue, K. A., Tracey, K. L., Watts, D. R., Chidichimo, M. P., & Chereskin, T. K. (2016). Mean Antarctic Circumpolar Current transport measured in Drake Passage. *Geophysical Research Letters, 43*(22), 11760–11767. https://doi.org/10.1002/2016GL070319

[5] Eyring, V., Bony, S., Meehl, G. A., Senior, C. A., Stevens, B., Stouffer, R. J., & Taylor, K. E. (2016). Overview of the Coupled Model Intercomparison Project Phase 6 (CMIP6) experimental design and organization. *Geoscientific Model Development, 9*, 1937–1958. https://doi.org/10.5194/gmd-9-1937-2016

[6] Ghil, M., Allen, M. R., Dettinger, M. D., Ide, K., Kondrashov, D., Mann, M. E., Robertson, A. W., Saunders, A., Tian, Y., Varadi, F., & Yiou, P. (2002). Advanced spectral methods for climatic time series. *Reviews of Geophysics, 40*(1), 1003. https://doi.org/10.1029/2000RG000092

[7] Grassberger, P., & Procaccia, I. (1983). Measuring the strangeness of strange attractors. *Physica D: Nonlinear Phenomena, 9*(1–2), 189–208. https://doi.org/10.1016/0167-2789(83)90298-1

[8] Hersbach, H., Bell, B., Berrisford, P., Hirahara, S., Horányi, A., Muñoz-Sabater, J., Nicolas, J., Peubey, C., Radu, R., Schepers, D., Simmons, A., Soci, C., Abdalla, S., Abellan, X., Balsamo, G., Bechtold, P., Biavati, G., Bidlot, J., Bonavita, M., De Chiara, G., Dahlgren, P., Dee, D., Diamantakis, M., Dragani, R., Flemming, J., Forbes, R., Fuentes, M., Geer, A., Haimberger, L., Healy, S., Hogan, R. J., Hólm, E., Janisková, M., Keeley, S., Laloyaux, P., Lopez, P., Lupu, C., Radnoti, G., de Rosnay, P., Rozum, I., Vamborg, F., Villaume, S., & Thépaut, J.-N. (2020). The ERA5 global reanalysis. *Quarterly Journal of the Royal Meteorological Society, 146*(730), 1999–2049. https://doi.org/10.1002/qj.3803

[9] Jungclaus, J. H., Lorenz, S. J., Schmidt, H., Brovkin, V., Brüggemann, N., Chegini, F., Crüger, T., De-Vrese, P., Gayler, V., Giorgetta, M. A., Gutjahr, O., Haak, H., Hagemann, S., Hanke, M., Ilyina, T., Kornblueh, L., Kröger, J., Linardakis, L., Mehlmann, C., Mikolajewicz, U., Müller, W. A., Nabel, J. E. M. S., Notz, D., Pohlmann, H., Putrasahan, D. A., Raddatz, T., Ramme, L., Redler, R., Reick, C. H., Riddick, T., Sam, T., Schneck, R., Schnur, R., Schupfner, M., von Storch, J.-S., Wachsmann, F., Wieners, K.-H., Ziemen, F., Stevens, B., Marotzke, J., & Claussen, M. (2022). The ICON Earth System Model version 1.0. *Journal of Advances in Modeling Earth Systems, 14*(4), e2021MS002813. https://doi.org/10.1029/2021MS002813

[10] Kantz, H., & Schreiber, T. (2003). *Nonlinear time series analysis* (2nd ed.). Cambridge University Press.

[11] Lorenz, E. N. (1963). Deterministic nonperiodic flow. *Journal of the Atmospheric Sciences, 20*(2), 130–141. https://doi.org/10.1175/1520-0469(1963)020<0130:DNF>2.0.CO;2

[12] North, G. R., Bell, T. L., Cahalan, R. F., & Moeng, F. J. (1982). Sampling errors in the estimation of empirical orthogonal functions. *Monthly Weather Review, 110*(7), 699–706. https://doi.org/10.1175/1520-0493(1982)110<0699:SEITEO>2.0.CO;2

[13] Rosenstein, M. T., Collins, J. J., & De Luca, C. J. (1993). A practical method for calculating largest Lyapunov exponents from small data sets. *Physica D: Nonlinear Phenomena, 65*(1–2), 117–134. https://doi.org/10.1016/0167-2789(93)90009-P

[14] Rosso, O. A., Larrondo, H. A., Martin, M. T., Plastino, A., & Fuentes, M. A. (2007). Distinguishing noise from chaos. *Physical Review Letters, 99*(15), 154102. https://doi.org/10.1103/PhysRevLett.99.154102

[15] Takens, F. (1981). Detecting strange attractors in turbulence. In D. Rand & L.-S. Young (Eds.), *Dynamical systems and turbulence, Warwick 1980* (Lecture Notes in Mathematics, Vol. 898, pp. 366–381). Springer. https://doi.org/10.1007/BFb0091924

[16] Theiler, J. (1986). Spurious dimension from correlation algorithms applied to limited time-series data. *Physical Review A, 34*(3), 2427–2432. https://doi.org/10.1103/PhysRevA.34.2427

[17] Vautard, R., & Ghil, M. (1989). Singular spectrum analysis in nonlinear dynamics, with applications to paleoclimatic time series. *Physica D: Nonlinear Phenomena, 35*(3), 395–424. https://doi.org/10.1016/0167-2789(89)90077-8